Article

Journal of the Brazilian Chemical Society

https://dx.doi.org/10.21577/0103-5053.20240161

J. Braz. Chem. Soc. **2025**, *36*, 3, e-20240161, 1-13

Natural Products Diversity from Genus *Aspergillus*: A Bioinformatics Study for Insecticidal Activity against the *Aedes aegypti* Vector

Inana F. de Araújo,[a] Ryan S. Ramos,[b] Mateus J. S. Matos,[a] Cleydson B. R. dos Santos,[b] Maryam Rameshrad,[c] Raimundo N. P. Souto[d] and Irlon M. Ferreira *,[a]

[a]*Laboratório de Biocatálise e Síntese Orgânica Aplicada, Universidade Federal do Amapá, 68903-419 Macapá-AP, Brazil*

[b]*Laboratório de Modelagem e Química Computacional, Departamento de Ciências Biológicas e Saúde, Universidade Federal do Amapá, 68903-419 Macapá-AP, Brazil*

[c]*Department of Electronics and Information Engineering, Jeonbuk National University, Jeonju, 54896 South Korea*

[d]*Laboratório de Artrópodes, Departamento de Biologia, Universidade Federal do Amapá, 68903-419 Macapá-AP, Brazil*

Computational predictive approaches present themselves as an attractive alternative in the search for new compounds that may present toxic or growth regulatory activity in *Aedes aegypti*. *Aspergillus* species is a producer of secondary metabolites with diverse biological activities. In this study, it was possible to evaluate the pharmacokinetic and toxicological properties *in silico*, as well as the prediction of the insecticidal biological activities of the juvenile hormone of natural substances produced by the genus *Aspergillus*. Initially, 187 molecules were cataloged from various species of *Aspergillus* spp., and only seven molecules of indole alkaloids were found to exhibit a toxic dose 50% (TD_{50}) after conducting toxicity predictions. The molecular dynamic simulation trajectories were utilized to study parameters such as root mean square deviation, root mean square fluctuation, radius of gyration and intermolecular hydrogen bond to understand the behavior and stability of proposed compounds in the binding pocket of the target protein. The *N*-β-acetyltryptamine molecule showed a binding affinity value of –8.100 ± 0.200 kcal mol^{-1}, which classifies the compound as a potential insecticidal agent against the *Aedes aegypti* vector.

Keywords: Amazonian biodiversity, *Aspergillus*, molecular dynamic simulation, toxicological properties

Introducion

Aedes aegypti mosquito (Diptera: Culicidae) is one of the most studied vector species worldwide, implying the transmission of pathogens responsible for the transmission of diseases to humans, such as dengue, Chikungunya, Zika, yellow fever, and the set of its physiological and genetic characteristics allow this species to be an extremely efficient vector.[1]

The more efficient chemical control of mosquitoes has been carried out mainly by combating the vector larvae.[2] However, the irrational and intensive use of these chemical agents has caused serious environmental and human health impacts, in addition, to creating resistant populations of mosquitoes.[3] The search for new chemical entities with less toxicity to the environment and the health of the human population involves extensive investigations and, in some cases, optimization of the cost of research, when looking for new pesticides with different modes of action, and that have less impact on the health of organisms not targeted for public health use.[1,4]

Microorganisms, such as fungi and bacterium, are also font for new molecules with larvicidal activity. Among the most fungal genera, the *Aspergillus* spp stands out as a capacity producer of secondary metabolites including butenolides, alkaloids, terpenoids, cytochalasin's, phenalene's, ρ-terphenyls, xanthones, sterols, diphenyl

*e-mail: irlon.ferreira@gmail.com
Editor handled this article: Paula Homem-de-Mello (Associate)

ether, sesquiterpenoid,[5] and anthraquinone derivatives and other diverse biological activities,[6] as antibiotics and antifungal agents, synthase and α-glucosidase inhibitor.[7-9] *Aspergillus* is one of the most familiar filamentous fungi belonging to Ascomycetes (family Trichocomaceae). There are about 378 species reported by the World of Microorganisms Information Center (WDCM).[10,11] Furthermore, the genus *Aspergillus* comprises the most ubiquitous and best studied filamentous fungi, being a species of industrial importance that can be harmful or opportunistic pathogens that secrete potent toxins.[12]

The evolution of secondary metabolites over the years was attibuted to the relationship of microorganisms with their habitat, using these substances as chemical signals for communication, habitat defence and even inhibiting the growth of competitor agents. Fungi have become capable of producing numerous bioactive compounds such as indole alkaloids, with low molecular weight and these products have been of great interest in food, cosmetics, and pharmaceutical industries.[13,14] These alkaloids have gained attention in biological studies, due to their structure and varied biological responses, as several studies[15-17] have reported the production of these substances by microorganisms, such as fungi of the genus *Aspergillus* and *Penicillium.* Produced metabolites of the alkaloid class are abundant and complex, existing from natural products, presenting a fascinating structure for the development of new drugs.

Aspergillus spp has the ability to produce metabolites that exhibit a promising diversity in chemistry and bioactivity.[18,19] The search for new biotechnological applications for the metabolites has become the target of research to control vectors such as *Ae. aegypti* and *Culex quinquefasciatus*,[6,20,21] biodegradation of polluting substances,[22] anticancer and antitrypanosomal activity.[23]

Although natural products are treated as a valuable source for the discovery of new substances,[6,24] their isolation and chemical characterization is not always feasible, as it is an expensive, slow, and costly process.[25] In this sense, molecular modelling and high-throughput screening techniques are complementary tools that gain attention and drive the development of new active compounds.[26]

One advantage of the computational method for the development of new substances is the expansion of the toxicological and chemical database in recent years, thus increasing the reliability of the *in silico* approach to toxicity assessment.[4] The use of the *in silico* approach for the discovery of new substances or similar compounds that present biological activity for the control of *Ae. aegypti* is already a reality. For example, pyriproxyfen (control compound) was studied by Ramos *et al*.,[27] for insecticidal activity by interaction with the enzyme acetylcholinesterase (AChE), in which the compound ZINC00001624 showed potential for enzyme inhibition AChE and for the juvenile hormone, showing promise for future studies.

Therefore, this study sought to evaluate, through molecules produced and isolated from the fungus of the genus *Aspergillus*, the potential insecticidal activity against the vector *Ae. aegypti* via virtual screening, as well as evaluating the pharmacokinetic and toxicological properties *in silico*, and the prediction of the insecticidal biological activities of the juvenile hormone, followed by the molecular docking study to evaluate the free energy of binding and the mode of interaction of the compounds described already in the literature.

Experimental

Obtaining, optimizing and molecular docking for selected structures

Initially, 187 chemical structures described in the literature as substances identified by the metabolic expression of the fungi genus *Aspergillus* were selected (presented in Supplementary Information (SI) section).[28,29] Structures were drawn in ChemDraw Ultra 12.0 software[30] and saved in MDL Molfile (.mol) format. Then, the geometric optimization of the three-dimensional (3D) structure was performed in the software ChemSketch[31] by Molecular Mechanics (MM^+) method with the force field initially based on the CHARMM parameterization.[32]

Prediction of pharmacokinetic and toxicological properties

Calculations of predictions of absorption, distribution, metabolism, excretion, and toxicity (ADMET) were performed using Discovery Studio v.16 software.[33] These properties are important in determining the success of the compound for human therapeutic use. Some important chemical descriptors correlate well with ADMET properties, such as polar surface area (PSA) as primary determinant of fraction absorption and low molecular weight (MW) for oral absorption and instestinal. The distribution of compounds in the human body depends on factors such as the blood-brain barrier logarithm (log BBB), permeability such as Caco-2 apparent permeability, Madin-Darby canine kidney (MDCK) cell apparent plasma proteins logarithm (log Khsa for protein binding).

Toxicity prediction tests were performed using Discovery Studio v.16 software[33] via the toxicity prediction

function by computer assisted technology (TOPKAT). In this way, the module can predict the toxicity of chemicals based solely on their 2D molecular structure, using a variety of robust cross-validated quantitative structure-toxicity relationship (QSAR) models to evaluate specific toxicological parameters. The proven toxicological properties were: carcinogenicity in rodents (female mice and female rats) and Ames test (mutagenicity), toxicity risk prediction calculations were performed via TOPKAT and measured the following parameters: oral rate lethal dose (LD_{50} g kg^{-1} body weight) and carcinogenic potential was also predicted using toxic dose (TD_{50} mg kg^{-1} body weight mouse-day^{-1} rat) and RMTD (maximum tolerated dose in rat mg kg^{-1} body weight).

Molecular docking simulations

At this step, only the top-ranked molecules with satisfactory results regarding the pharmacokinetic, toxicological, and biological activity predictions were selected for the molecular docking simulations, in order to evaluate the energy function scores through the free energy value (ΔG) of the interaction of ligands derived from the ligand-based virtual screening, as well as analysis of the conformations and binding affinity mode with the targets used here.

Selection of enzyme and inhibitor structures

As insecticides can act in different sites, the two pathways of action mechanism are the highlights: juvenile hormone (JH3) enzymes and acetylcholinesterase. Similarly, JH3 is a key regulation of insect development and breeding. In adult mosquitoes, it is essential for ovary maturation and normal male reproductive behavior, but how the distribution and activity of JH3 are regulated is unclear after secretion. The crystallographic structure of juvenile hormone complexed with methyl (2*E*,6*E*)-9-[(2*R*)-3,3-dimethyloxiran-2-yl]3,7-dimethylona-2-6-dienoate, (JH3), was downloaded with the Protein Data Bank PDB ID 5V13[34] and 1.87 Å resolution.[35] The JH3 compound was used here as a control inhibitor in the molecular docking studies, based on a well-established protocol developed.[6,36]

Docking study from AutoDock 4.2/Vina

Heteroatoms, co-crystallized ligand, and water molecules were removed using the Discovery Studio software,[33] while the hydrogen atoms of the proteins were added with PROPKA using pH ca. 7. The validation of molecular docking protocols was performed by overlapping the elucidated crystallographic structure (experimental) with the generated model (theoretical), that is, comparison between the crystallographic ligand and the best conformation obtained with molecular docking based on the value of the root mean square deviation (RMSD). Coordinates x, y, and z of the receptors were determined according to the middle region of the active site. The coordinates used here for the center of the grid can be seen in Table 1. An energy function score was used to evaluate the binding free energy (ΔG) of the interaction of the ligands with the amino acid residues of the receptors. The conformational analysis was also considered for the selection of the best binding free energy for binding affinity calculations via AutoDock 4.2/Vina 1.1.2.[37] Visualizations as well as distance measures of interactions between inhibitors and enzymes were performed using Discovery Studio.[33]

Molecular dynamic simulation method

Molecular dynamics (MD) simulation[38] is a computational technique used for studying the interaction and behavior of small molecules over a specific time. In this study, molecular dynamic simulation of the target protein (5V13)[39] in complex with top screened compounds and controls was performed using Molecular Dynamics Software NAMD tool (version 2.14)[40] and Amber tools platform.[41] The purpose of this study was to analyze and compare the binding strength of the screened compounds and control compounds within the binding site of the 5V13.

The tLeap module[42] from Amber tools[41] were utilized to generate the protein and ligand forcefield FF14SB,[43] GAFF[44] respectively, and construction of input files for the NAMD tool[40] MD simulations. TIP3P solutions were employed to solvate the complexes in a periodic, cubic box by 10 Å beyond each protein atom. Counter ions such as Na^+, Cl^- were added for system neutralization. Furthermore,

Table 1. Data from protocols used for molecular docking validation on Protein Data Bank (PDB) ID 5V13

Enzyme (PDB ID 5V13)	Ligand	Grid coordinates	Grid dimensions
Juvenile hormone	methyl (2*E*,6*E*)-9-[(2*R*)-3,3-dimethyloxiran-2-yl]-3,7-dimethylnona-2,6-dienoate	X = 238.978	34 x
		Y = –26.138	30 y
		Z = 353.063	26 z

particle meh Ewald (PME) method was employed to calculate the electrostatic interactions, Varlet method with cutoff 10 Å was used for calculating electrostatic interactions and Van der Waals interactions, while bond constrained were managed using linear constrained solver (LINCS) algorithm.[45]

In MD simulation, the system achieved multiple phases to reach equilibrium. In this first step, steepest descent algorithm was used to minimize the system up to 10,000 steps. The system was heated up to 300 K for 0.10 ns with gradually increased up to 50 K. Berendsen thermostat was used to manage the temperature and Langevin piston for pressure control of the system. The temperature and pressure of the system were kept constant at 1 bar and 300 K for 100 ns production run. Moreover, particle mesh Ewald (PME) method was choice for handling long electrostatic interactions during simulation in periodic boundary condition.[46]

Subsequently, MD trajectories were analyses using visual molecular dynamics (VMD),[47] Cpptraj[48] and R package.[49] The evaluating parameters such as root mean square deviation (RMSD), root mean square fluctuation (RMSF), radius of gyration and hydrogen bond trajectory were evaluated. The evaluation of these parameters was crucial to assessing the stability of the target protein and small molecules throughout the molecular dynamics (MD) simulation.[50]

Binding free energy calculation

The binding free energy of the complexes was calculated by using molecular mechanics-based method (MMGBSA).[51] For this purpose, 300 snapshots of the complex captured at 2 ps intervals from the final 2 ns of the stable MD trajectories were utilized for MMGBSA calculations. The binding free energy calculation is determined by taking the difference between the ligand and target protein $\Delta G_{complex}$ total free energy and the sum of the individual free energy of the receptor $\Delta G_{protein}$ and ligand ΔG_{ligand} as expressed in following equations 1 and 2:

$$\Delta G_{bind} = [\Delta G_{complex} - (\Delta G_{protein} + \Delta G_{ligand})] \quad (1)$$

Whereas $\Delta G_{complex}$ is the combination of the following energies:

$$\Delta G_{complex} = [\Delta G_{MM} + \Delta G_{solvation} - T\Delta S] \quad (2)$$

where: ΔG_{MM} = molecular mechanics energy, $\Delta G_{solvation}$ = solvation energy, and $T\Delta S$ = entropy value at temperature T.

Results and Discussion

Pharmacokinetic and toxicological predictions

Calculated topological polar surface area (TPSA) values of the molecules are within acceptable limits, less than 140 Å.[52-54] Thus, the distribution of molecules in the human body, as indicated by the blood-brain barrier coefficient logarithm (logBBB), Caco-2 apparent permeability, logKp for skin permeability, the volume of distribution and binding to plasma proteins logarithm (log Khsa for whey protein binding) were determined in the standard range.[55] After application of the screening filters, 22 molecules have good aqueous solubility, and the others have low solubility (Figure 1). The calculated logS values of the molecules are within the acceptable range (≥ –5) and conform to the standard absorption, distribution, metabolism, and excretion (ADME) range. The molecules were compared to the reference ligand, and it was observed that most molecules are within their allowable limits and are therefore unlikely to have limited bioavailability.

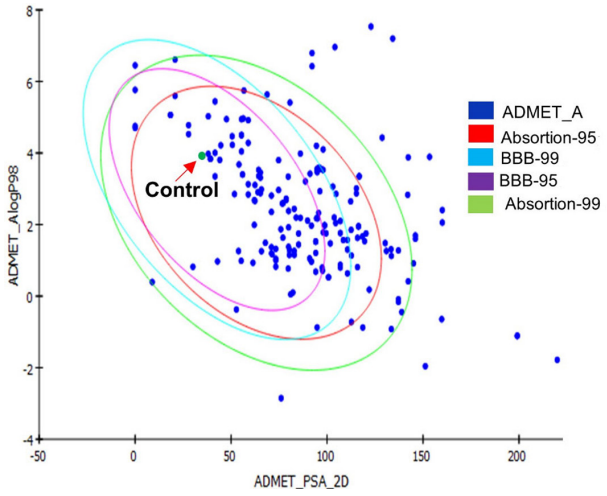

Figure 1. The plot of polar surface area (PSA) *versus* logAP for molecules isolated from different *Aspergillus* species shows the ellipses of the 95 and 99% confidence limits corresponding to the blood-brain barrier (BBB) and intestinal absorption (IA).

The results of the screening of molecules in the ADME model showed that of the 187 molecules and controls submitted to pharmacokinetic prediction, only 39 have 99% confidence levels for human intestinal absorption and low penetration into the BBB. The other molecules are outside the ellipse filter of the ADME model, which indicates the low intestinal absorption and greater penetration capacity of BBB. Toxicity is a major obstacle to successful drug discovery and development. In recent years, this has led to an increasing focus on high-throughput studies of ADME and toxicity.[56,57]

TOPKAT model calculates likely toxicity values for a chemical structure by calculating a discriminant score based on its quantitative structure-activity relationship (QSAR) model.[57,58] Molecules with a good pharmacokinetic profile were submitted to the study of toxicological predictions. Based on chemical structures, the discriminant score of 12 molecules was negative, indicating their non-carcinogenic property. Likewise, the 12 molecules did not show mutagenicity. These molecules conform to parameters based on the pivot molecule and are comparable to the predicted results of the reference compounds.

All selected compounds (Table 2) showed a negative prediction for carcinogenicity (rat/mouse model and the Ames test), which highlights the possible absence of toxicophoric groups. However, a carcinogenicity alert was observed for the pivot molecule. Regarding carcinogenic potency, only 7 molecules present TD_{50} values higher than the reference TD_{50} molecule of 54.8404 (mg kg^{-1} body weight day^{-1}), which highlights a low toxicity profile of the selected molecules (Table 2).

Currently, the most used assay to test the mutagenicity of compounds is the Ames experiment. The Ames test is a short-term bacterial reverse mutation assay that detects a significant number of compounds that can induce genetic damage and frame-shift mutations (Figure 2). The estimated inter-laboratory reproducibility rate of *Salmonella* test data is only 85%.[59,60]

Molecular docking

The molecular docking results were considered satisfactory since the relative pose of the crystallographic ligand and the pose docking were considered similar. The root mean square deviation (RMSD) value between the

Table 2. Predictions of toxicological properties of selected molecules and carcinogenic potency TD_{50} (toxic dose 50%)

Ligand	Carcinogenic potency, TD_{50} / (mg kg^{-1} body weight day^{-1})				
	Mouse	Rat	Maximum tolerated dose	Mouse female / Rat female	Ames mutagenicity
Juvenile hormone (JH3)	39.6698	13.9437	54.8404	non-carcinogen / single-carcinogen	non-mutagen
Aniquinazoline B	17.5998	0.363458	56.6879	non-carcinogen	non-mutagen
Aspergilline E	12.1197	0.070666	44.7533	non-carcinogen	non-mutagen
bis(Dethio)bis	155.878	172.44	59.928	non-carcinogen	non-mutagen
Carnemycin A	51.4169	24.8186	2526.16	non-carcinogen	non-mutagen
Carnemycin B	52.0468	6.63612	1463.3	non-carcinogen	non-mutagen
Fumigatoside C	0.85852	0.040724	63.3249	non-carcinogen	non-mutagen
Fumigatoside D	0.85852	0.040724	63.3249	non-carcinogen	non-mutagen
N-β-Acetyltryptamine	515.893	678.596	253.885	non-carcinogen	non-mutagen
Oxepinamide F	16.3633	6.23257	21.5888	non-carcinogen	non-mutagen
Oxepinamide G	15.514	7.97591	15.7309	non-carcinogen	non-mutagen
Protuboxepin A	10.7233	4.90675	35.7106	non-carcinogen	non-mutagen
Protuboxepin B	10.1355	6.26023	25.9517	non-carcinogen	non-mutagen

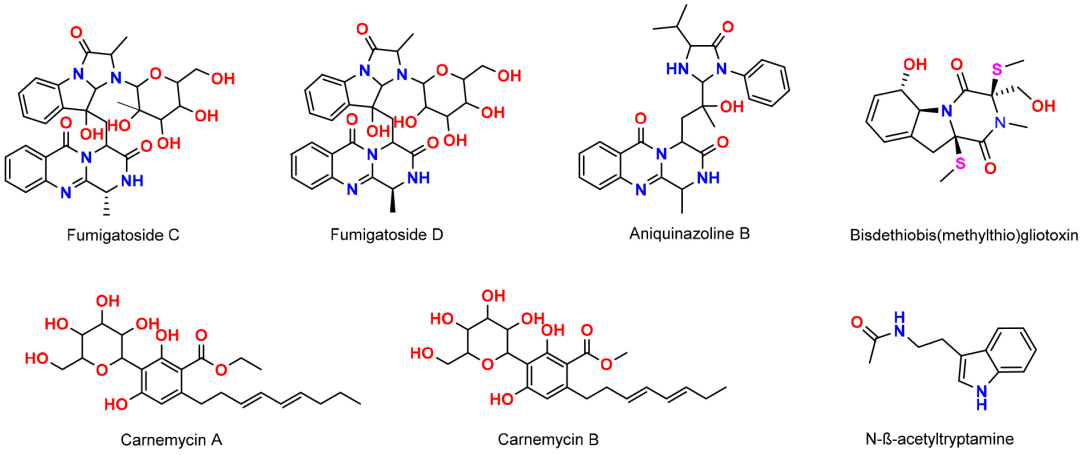

Figure 2. Chemical structure of secondary metabolites from *Aspergillius* spp.

JH3 crystallographic ligand atoms and the docking pose was calculated to be 1.43 Å.

Thus, the literature[61,62] specifies that when the RMSD values ≤ 2 Å, the docking protocol is considered satisfactory because it presents a similarity to the experimental model. The best result of the experimental (crystallographic ligand) and theoretical (docking pose) overlay models can be seen in Figure 3.

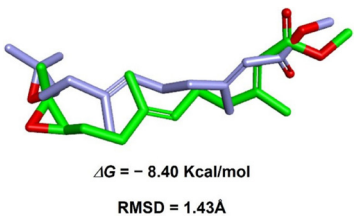

Figure 3. Superimposition of molecular docking (green) and crystallographic ligand (blue) poses.

According to studies of Araújo *et al.*,[6] and Ramos *et al.*,[27] at the juvenile hormone binding site, interactions are between the amino acid residues Leu33-Leu37, Ile44-Val51, Tyr59-Glu71, and Cys122-His136 in the α-helix and interactions between the Leu72-Arg73 residues in the β-leaf.[63] Interactions observed in the molecules selected in the molecular docking study are classified as being of the hydrophobic type in their majority, and the interactions of the hydrogen bond type are less frequent. Interactions were quantified for binding affinity relative to control (JH3) for the mosquito juvenile hormone-binding protein and the new potential inhibitors. The affinity values of the new potential inhibitors can be seen in Figure 4.

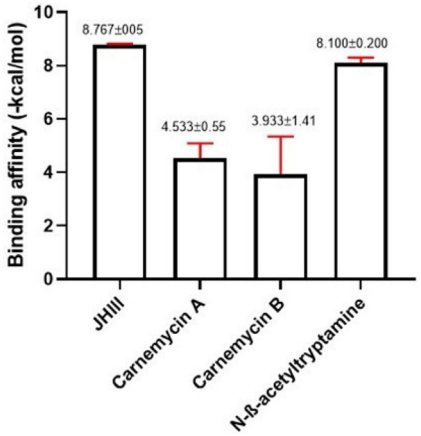

Figure 4. Binding affinity values of potential ligands with the juvenile hormone receptor (p value < 0.0001; n = 3).

The difference between the binding affinity values between the *N*-β-acetyltryptamine inhibitor and the JH3 control was ± 0.667 kcal mol^{-1}, which classifies the compound as a potential insecticidal agent, as it may have a similar interaction in the receptor causing a delay in the growth process or morphological malformation and cause the death of the *Ae. aegypti*.

In the mosquito juvenile hormone-binding protein receptor complexed with JH3, similar interactions were observed with the molecules carnemycin A, carnemycin B and *N*-β-acetyltryptamine present between the amino acid residues around the α-helix between the amino acid residues Tyr33, Leu37, Val51, Val68, and Tyr129 and in the β-leaf between residues Trp53 and Phe144, as shown in Figure 5.

The epoxy group at the end of JH3 forms a hydrogen bond with the phenolic hydroxyl of Tyr129, and the remainder of the isoprenoid chain is surrounded by hydrophobic side chains, including those of Phe144, Tyr64, Trp53, Val65, Val68, Leu72, Leu74, Val51 and Tyr33.[64,65]

In the *N*-β-acetyltryptamine ligand with the best binding affinity results, it is possible to observe hydrophobic interactions with the amino acid residues Trp50, Trp53, Val68, Tyr129 and Phe144. Conventional hydrogen bond between residues Trp50 and Val65 provides greater stability of the ligand and lower energy expenditure with the obtained conformation, which intensifies the biological activity in the active site. Studies[65,66] suggest that the greater stability of molecules at the binding site in the juvenile hormone receptor is attributed to hydrogen bond interactions, due to the presence of water residues in the protein, which corroborates the study, since the potential molecule presents interactions of the hydrogen bond type. Consequently, potential insecticidal agents can prevent mosquitoes from molting from pupae to adults by mimicking the action of their natural juvenile hormones.

Juvenile hormone (JH) is a key regulator of insect development and reproduction.[67,68] The physiological activity of the mosquito juvenile hormone binding protein (mJHBP) has not yet been established, and it may act in the regulation of JH concentration in the hemolymph.[64] Regulators of mosquito physiology are obvious targets in the development of control agents against these parasitic and viral disease vectors that threaten a large fraction of the human population.

Post molecular dynamics simulation analysis

The molecular dynamic simulation trajectories were utilized to study parameters such as RMSD, RMSF, radius of gyration and intermolecular hydrogen bond to understand the behavior and stability of proposed compounds in the binding pocket of the target protein. The root mean square deviation (RMSD) was calculated for each compound as

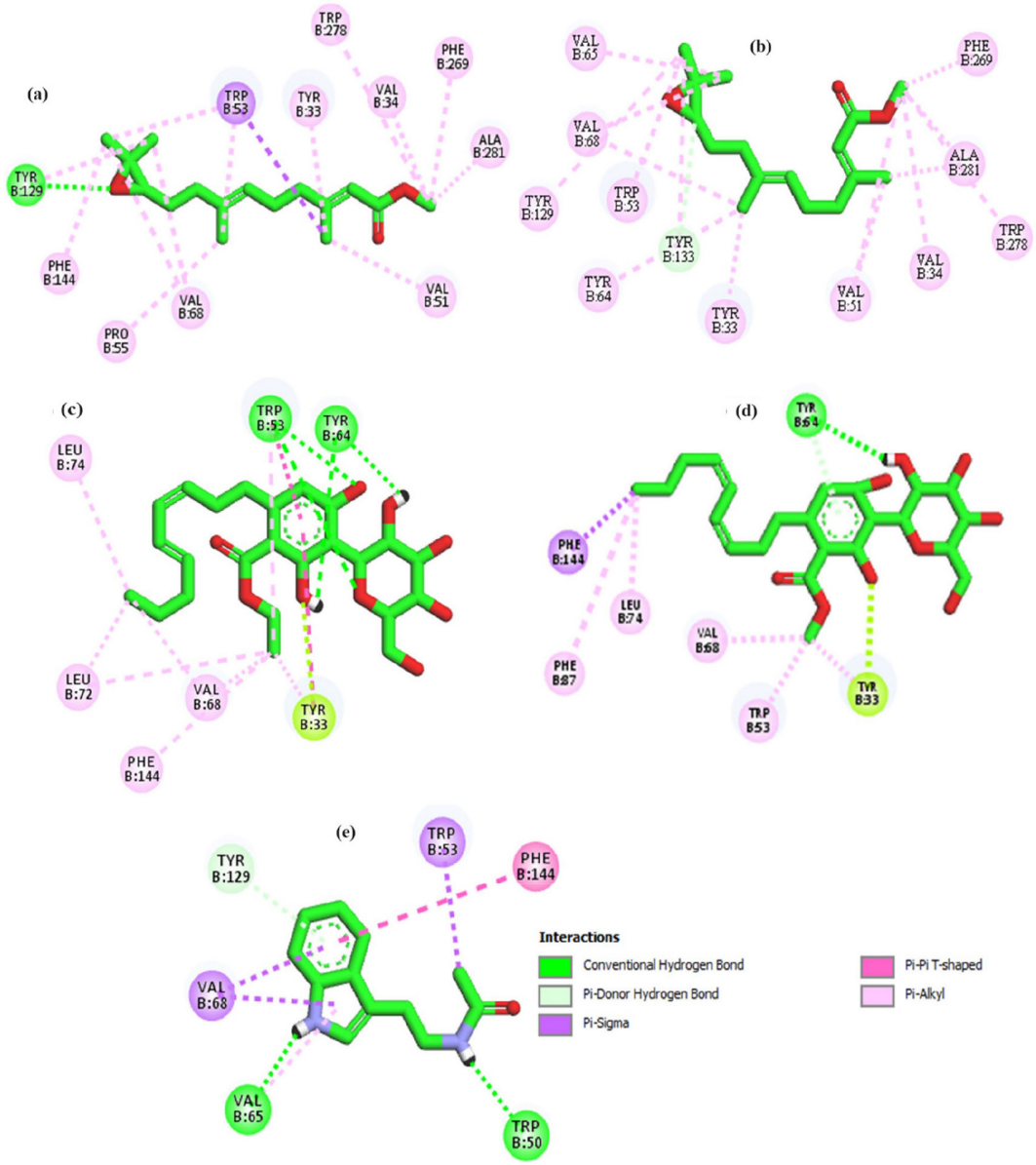

Figure 5. Interactions of controls JH3 (a), JH3 docking pose (b), potential larvicidal agents carnemycin A (c), carnemycin B (d) and *N*-β-acetyltryptamine (e) at the binding site.

shown in Figure 6 from the starting to the end frame during the whole production run. The average RMSD value for compound 11NBA (*N*-β-acetyltryptamine) was 1.5 Å, 103 (carnemycin B) was 1.4 Å, 435_h (carnemycin A) was 1.6 Å and JH3 was 1.4 Å. The relationship between the average RMSD values and the stable conformations of the modeled compounds showed direct proportions in the graph curve. The graph illustrates that 11NBA attained equilibrium from 20 ns, whereas other compounds 103, 435_h and control compound (JH3) reached at steady-state from 10 ns. Moreover, the plateau comparison of proposed compounds indicates that compounds 103 and 435_h exhibit comparable behavior with control compounds (Figure 6).

Furthermore, RMSF fluctuations were observed in all compounds in Figure 7, showing no significant variation with their time-averaged values. There are some residues such as Leu267, Asp208, Ala210, Ala207, Glu1 that fluctuated more during the production run. However, these residues are present at the N and C terminal of the target protein and do not involve in the interaction of the small molecules in the binding site of the protein. In contrast, there was also minimal fluctuation at the residue Asn166 which is a part of loop region and does not affect binding of compounds with the protein. When compounds were compared to the control compound JH3, it was found that compound 103 exhibited better stability and binding in the same way as control compound (Figure 7).

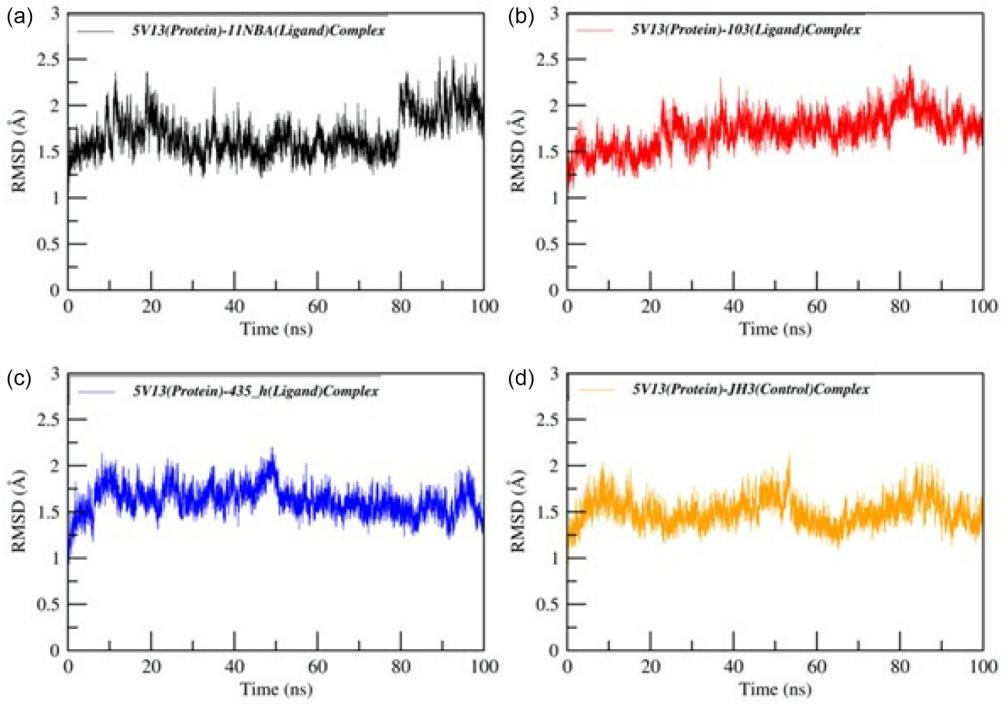

Figure 6. Root mean square deviation (RMSD) plot illustration throughout protein in complex with ligand simulations at 100 ns. (a) 5V13-11NBA (*N*-β-acetyltryptamine), (b) 5V13-103 (carnemycin B), (c) 5V13-435_h (carnemycin A) and (d) 5V13-JH3 (control) complexes.

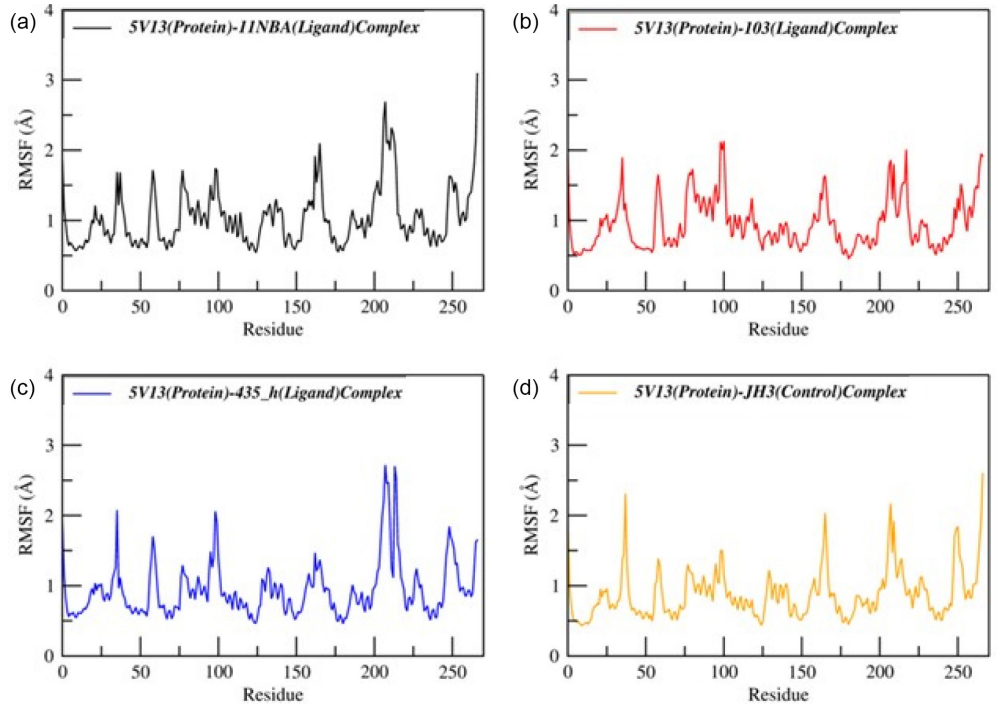

Figure 7. Root mean square fluctuation (RMSF) plot illustration throughout protein in complex with ligand simulations at 100 ns. (a) 5V13-11NBA (*N*-β-acetyltryptamine), (b) 5V13-103 (carnemycin B), (c) 5V13-435_h (carnemycin A) and (d) 5V13-JH3(control) complexes.

For instance, radius of gyration graph represented in Figure 8, shows the consistency of protein during simulation time. If a protein is efficiently folded during its interaction with small molecule, a relatively steady radius of gyration plot is achieved. We observed that radius of gyration of protein is stable and compact in the complex with JH3, 103 and 435_h compared with the control compound. The average radius of gyration ranges from 16 to 20 Å showing the nominal spatial distribution of atoms within the molecule.

The stability of the protein was also assessed with the hydrogen bond calculations between their atoms. The average hydrogen bond count for JH3, 103, 435_h and the control compound was 70 ns during simulation time. All proposed small molecules exhibited a high number of hydrogen bonds, with consistent intra-molecular bond formation, indicating the strong interactions between the residues of the protein (Figure 9).

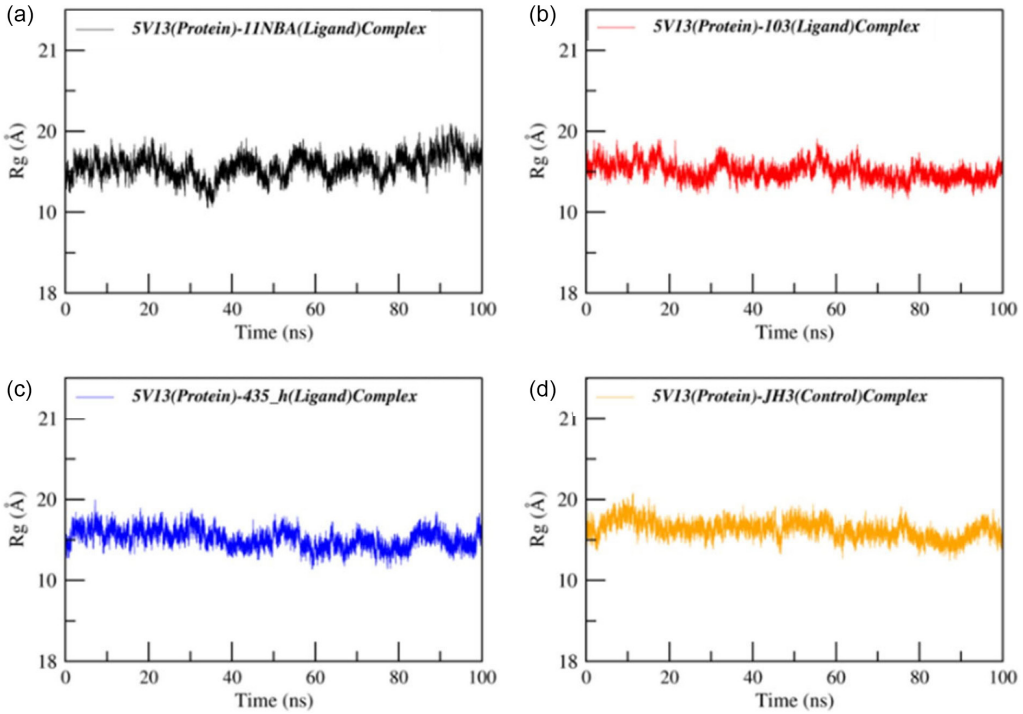

Figure 8. Radius of gyration plot illustration throughout protein in complex with ligand simulations at 100 ns. (a) 5V13-11NBA (*N*-β-acetyltryptamine), (b) 5V13-103 (carnemycin B), (c) 5V13-435_h (carnemycin A) and (d) 5V13-JH3(control) complexes.

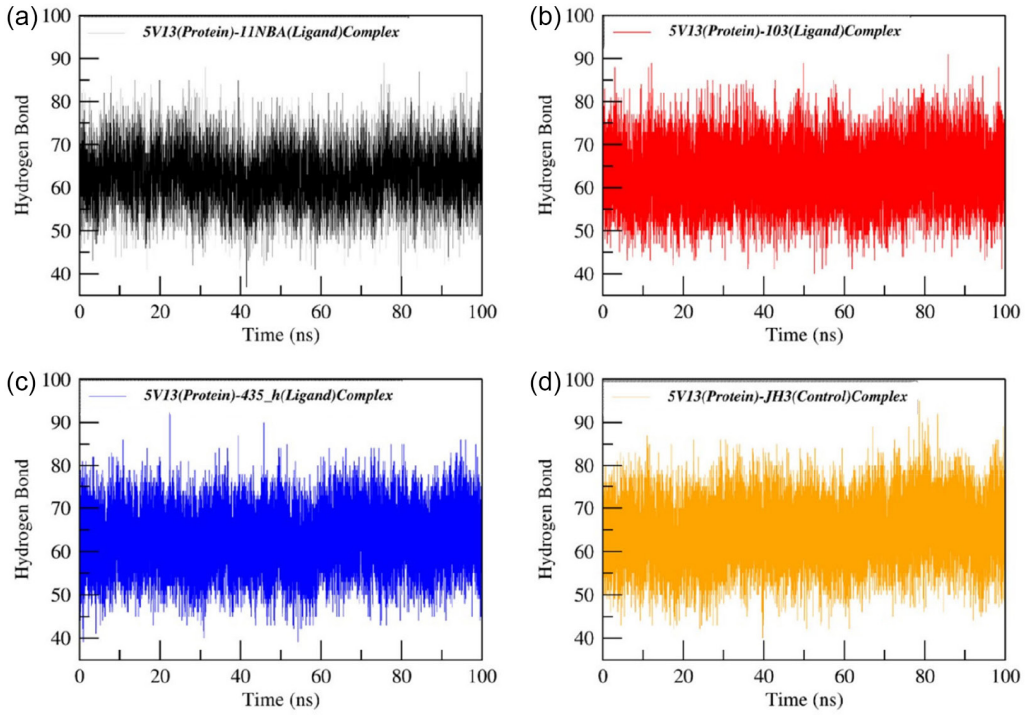

Figure 9. The number of hydrogen bonds that are created during simulation between a binding site of the protein and top screened and control compound: (a) 5V13-11NBA (*N*-β-acetyltryptamine), (b) 5V13-103 (carnemycin B), (c) 5V13-435_h (carnemycin A) and (d) 5V13-JH3(control). The plots demonstrate how every complex exhibits constant hydrogen bonding.

Binding free energy interpretation

The molecular mechanics generalized born surface area (MMGBSA) method was employed to compute the binding free energy calculation of best screened and control compounds. Binding free energy serves as a significant indicator to predict the binding affinity of the protein-ligand complexes, more negative values demonstrate greater stability.[69] The calculation of total energy is a combination of interactions such as Van der Waals energy (VDW), electrostatic energy (EEL), electrostatic potential-based (EPB), polar solvation energy (ENPOLAR), and dispersion energy (EDISPER), shown in Table 3. The average ΔG_{total} of the compound JH3, 103, and 435_h was –37.8724, –54.1922, and –64.9947 kcal mol^{-1}, respectively. The ΔG_{total} value of compound 435_h is much higher than control compound JH3 –41.1650 kcal mol^{-1} exhibited better binding affinity with target protein (Table 3).

The role of each amino acid of the simulated complexes in binding free energy calculation was investigated by decomposition analysis. According to Figure 10, a total of 5 residues whose positive energy contribution is equal and greater to –1 kcal mol^{-1} in hit and control compound includes Tyr14, Trp34, Val46, Val49, Tyr110. However, Tyr45 and Lys33 showed unfavorable interaction with 5V13-103 complex as it showed positive binding energy values. The high energy contribution of residue Tyr14 in 5V13-103, 5V13-435_h and 5V13-JH3 complexes is due to π-π interaction between them. Moreover, Trp34 also shows a high positive contribution to the 5V13-11NBA complex due to CH group of residue and O atom of ligand. Based on the above interactions between residues and ligand atom, the π-π, CH–O are the main interactive forces and binding between hit compounds and can act as a potential inhibitory against 5V13 protein target (Figure 10).

Table 3. Binding free energy calculation of top inhibitory and control compounds against target protein 5V13

Binding energy (ΔG) / (kcal mol^{-1})	11_NBA	103	435_h	JH3 (control)
ΔG_{Vdw}	–38.9182	–64.1027	–70.9539	–48.5548
ΔG_{Elec}	–13.0197	–20.8832	–17.9707	–150.0701
ΔG_{Gb}	18.2924	38.5867	38.0387	167.5409
ΔG_{Surt}	–4.2269	–7.7929	–37.7978	–28.9440
ΔG_{Gas}	–51.9379	–84.9859	–88.9245	–198.6249
ΔG_{Solv}	14.0655	30.7937	75.1807	190.0914
Total	–37.8724	–54.1922	–64.9947	–41.1650

11NBA: compound *N*-β-acetyltryptamine; 103: compound carnemycin B; 435_h: compound carnemycin A; JH3: juvenile hormone; ΔG_{Vdw}: Van der Waals energy; ΔG_{Elec}: electrostatic energy; ΔG_{Gb}: polar free energy; ΔG_{Surt}: solvent-accessible surface area; ΔG_{Gas}: gas phase interaction energy; ΔG_{Solv}: solvation energy.

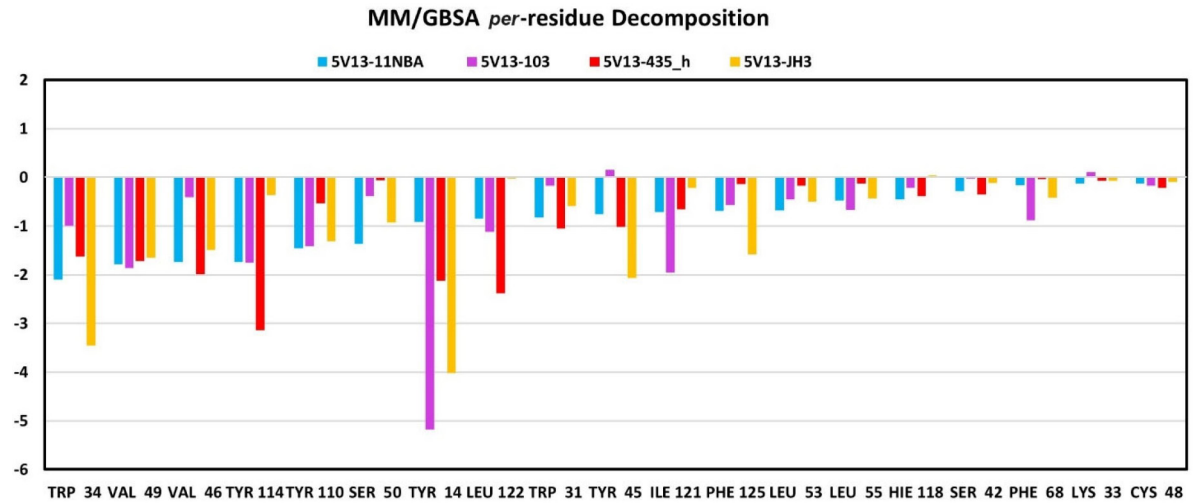

Figure 10. The residue contribution plot (MM-GBSA, molecular mechanics generalized born surface area), representing the binding contribution of residue in stabilizing the protein-ligand complexes.

Conclusions

A list of 187 compounds identified from different species of *Aspergillus* spp was related in this work to investigate the pharmacokinetic and toxicological properties *in silico*, for prediction of the insecticidal biological activities against *Ae. aegypti* vector. 39 molecules showed confidence levels for intestinal absorption and penetration into the blood-brain barrier, and a list with seven compounds demonstrated low toxicity profile, and the *N*-β-acetyltryptamine showed a binding affinity value of –8.100 ± 0.200 kcal mol^{-1}, for the juvenile hormone, which classifies the compound as a potential insecticidal agent against the *Aedes aegypti* vector. The results presented are considered satisfactory, and open interesting perspectives, with huge capacity of the *Aspergillus* genera as an attractive biological source that is worth further exploitation with distinguished anticipation for the global pharmaceutical and agrochemistry industries.

Supplementary Information

Supplementary information is available free of charge at http://jbcs.sbq.org.br as PDF file.

Acknowledgments

The authors acknowledge the Research Support Foundation of the State of Amapá (Fundação de Amparo à Pesquisa do Estado do Amapá, FAPEAP, grant No. 88887.568501/2020-00) and Coordination for the Improvement of Higher Education Personnel (CAPES) grant No. 88881.716142/2022-01 for financial support.

Author Contributions

Inana F. de Araújo was responsible for conceptualization, methodology, formal analysis, writing (original draft and editing); Ryan da S. Ramos for conceptualization, methodology, formal analysis, writing (original draft and editing); Mateus de J. S. Matos for methodology; Cleydson B. R. dos Santos for methodology, formal analysis, funding acquisition; Maryam Rameshrad for methodology, formal analysis, writing (original draft and editing); Raimundo N. P. Souto for writing (original draft and editing), funding acquisition; Irlon M. Ferreira for conceptualization, methodology, writing (original draft and editing), funding acquisition. All authors have read and agreed to the published version of the manuscript.

References

1. McGregor, B. L.; Connelly, C. R.; *J. Med. Entomol.* **2021**, *58*, 10. [Crossref]
2. Marinho, V. H. S.; Holanda, F. H.; Araújo, I. F.; Jimenez, D. E. Q.; Pereira, R. R.; Porto, A. L. M.; Ferreira, A. M.; Carvalho, J. C. T.; de Freitas, A. C. G. A.; Fernandes, C. P.; Souto, R. N. P.; Ferreira, I. M.; *Ind. Crops Prod.* **2023**, *203*, 117133. [Crossref]
3. Nkya, T. E.; Akhouayri, I.; Kisinza, W.; David, J. P.; *Insect Biochem. Mol. Biol.* **2013**, *43*, 407. [Crossref]
4. Santos, V. S. V.; Limongi, J. E.; Pereira, B. B.; *Chemosphere* **2020**, *247*, 125795. [Crossref]
5. Ingavat, N.; Mahidol, C.; Ruchirawat, S.; Kittakoop, P.; *J. Nat. Prod.* **2011**, *74*, 1650. [Crossref]
6. Araújo, I. F.; Marinho, V. H. S.; Sena, I. S.; Curti, J. M.; Ramos, R. S.; Ferreira, R. M. A.; Souto, R. N. P.; Ferreira, I. M.; *Biotechnol. Lett.* **2022**, *44*, 439. [Crossref]
7. Watanabe, S.; Hirai, H.; Ishiguro, M.; Kambara, T.; Kojima, Y.; Matsunaga, T.; Nishida, H.; Suzuki, Y.; Sugiura, A.; Harwood, H. J.; Huang, L. H.; Kojima, N.; *J. Antibiot.* **2001**, *54*, 904. [Crossref]
8. Satoi, S.; Yagi, A.; Asano, K.; Mizuno, K.; Watanabe, T.; *J. Antibiot.* **1977**, *30*, 303. [Crossref]
9. Mizuno, K.; Yagi, A.; Satoi, S.; Takada, M.; Hayashi, M.; Asano, K.; Matsuda, T.; *J. Antibiot.* **1977**, *30*, 297. [Crossref]
10. El-hawary, S. S.; Moawad, A. S.; Bahr, H. S.; Abdelmohsen, U. R.; Mohammed, R.; *RSC Adv.* **2020**, *10*, 22058. [Crossref]
11. Vadlapudi, V.; Borah, N.; Yellusani, K. R.; Gade, S.; Reddy, P.; Rajamanikyam, M.; Vempati, L. N. S.; Gubbala, S. P.; Chopra, P.; Upadhyayula, S. M.; Amanchy, R.; *Sci. Rep.* **2017**, *7*, 7325. [Crossref]
12. Scazzocchio, C. In *Encyclopedia of Microbiology*; Schmidt, T. M., ed.; Elsevier: Amsterdam, Netherlands, 2019. [Crossref]
13. Brakhage, A. A.; Schroeckh, V.; *Fungal Genet. Biol.* **2011**, *48*, 15. [Crossref]
14. Sarsaiya, S.; Jain, A.; Shi, J.; Chen, J. In *Biocontrol Agents and Secondary Metabolites*; Jogaiah, S., ed.; Elsevier: Amsterdam, Netherlands, 2021, ch. 1. [Crossref]
15. Félix, M. K. C.; Leite, E. R. T.; Dutra, L. R.; Ribeiro, M. A.; Moura, W. S.; Ferreira, T. P. S.; Santos, G. R.; Chapla, V. M.; Vieira, W. A. S.; Câmara, M. P. S.; Corrêa, M. J. M.; Viteri Jumbo, L. O.; Oliveira, E. E.; Cangussu, A. S. R.; *Ind. Crops Prod.* **2022**, *180*, 114743. [Crossref]
16. Li, S. M.; *Nat. Prod. Rep.* **2010**, *27*, 57. [Crossref]
17. Mitra, S.; Prova, S. R.; Sultana, S. A.; Das, R.; Nainu, F.; Emran, T. B.; Tareq, A. M.; Uddin, M. S.; Alqahtani, A. M.; Dhama, K.; Simal-Gandara, J.; *Phytomedicine* **2021**, *90*, 153649. [Crossref]
18. Luo, M. L.; Huang, W.; Zhu, H. P.; Peng, C.; Zhao, Q.; Han, B.; *Biomed. Pharmacother.* **2022**, *149*, 112827. [Crossref]
19. Zhao, W. Y.; Yi, J.; Chang, Y. B.; Sun, C. P.; Ma, X. C.; *Phytochemistry* **2022**, *193*, 113011. [Crossref]
20. Baskar, K.; Chinnasamy, R.; Pandy, K.; Venkatesan, M.; Sebastian, P. J.; Subban, M.; Thomas, A.; Kweka, E. J.; Devarajan, N.; *Heliyon* **2020**, *6*, e05331. [Crossref]

21. Bawin, T.; Seye, F.; Boukraa, S.; Zimmer, J. Y.; Raharimalala, F. N.; Ndiaye, M.; Compere, P.; Delvigne, F.; Francis, F.; *Fungal Biol.* **2016**, *120*, 489. [Crossref]
22. Holanda, F. H.; Birolli, W. G.; Morais, E. S.; Sena, I. S.; Ferreira, A. M.; Faustino, S. M. M.; Solon, L. G. S.; Porto, A. M.; Ferreira, I. M.; *Biocatal. Agric. Biotechnol.* **2019**, *20*, 101200. [Crossref]
23. Tawfike, A. F.; Romli, M.; Clements, C.; Abbott, G.; Young, L.; Schumacher, M.; Diederich, M.; Farag, M.; Edrada-Ebel, R. A.; *J. Chromatogr. B: Anal. Technol. Biomed. Life Sci.* **2019**, *1106*, 71. [Crossref]
24. Araújo, I. F.; de Araújo, P. H. F.; Ferreira, R. M. A.; Sena, I. D. S.; Lima, A. L.; Carvalho, J. C. T.; Ferreira, I. M.; Souto, R. N. P.; *S. Afr. J. Bot.* **2018**, *117*, 134. [Crossref]
25. Badawy, M. E. I. In *Studies in Natural Products Chemistry*; Rahman, A. U., ed.; Elsevier: Amsterdam, Netherlands, 2020, ch. 11. [Crossref]
26. Neto, R. A. M.; Santos, C. B. R.; Henriques, S. V. C.; Machado, L. O.; Cruz, J. N.; da Silva, C. H. T. P.; Federico, L. B.; de Oliveira, E. H. C.; de Souza, M. P. C.; da Silva, P. N. B.; Taft, C. A.; Ferreira, I. M.; Gomes, M. R. F.; *J. Biomol. Struct. Dyn.* **2022**, *40*, 2204. [Crossref]
27. Ramos, R. S.; Macêdo, W. J. C.; Costa, J. S.; da Silva, C. H. T. P.; Rosa, J. M. C.; da Cruz, J. N.; de Oliveira, M. S.; Andrade, E. H. A.; Silva, R. B. L.; Souto, R. N. P.; Santos, C. B. R.; *J. Biomol. Struct. Dyn.* **2020**, *38*, 4687. [Crossref]
28. Shi, Y. S.; Zhang, Y.; Chen, X. Z.; Zhang, N.; Liu, Y. B.; *Molecules* **2015**, *20*, 10793. [Crossref]
29. Soltani, J. In *New and Future Developments in Microbial Biotechnology and Bioengineering*; Gupta, V. K., ed.; Elsevier: Amsterdam, Netherlands, 2016, ch. 22. [Crossref]
30. *ChemDraw Ultra*, version 12.0; PerkinElmer, Waltham, MA, USA, 2020.
31. *Chemsketch Freware*, version 12.00; Advanced Chemistry Development, Inc., Toronto, Canada, 2010; Li, Z.; Wan, H.; Shi, Y.; Ouyang, P.; *J. Chem. Inf. Comput. Sci.* **2004**, *44*, 1886. [Crossref]
32. Brooks, B. R.; Bruccoleri, R. E.; Olafson, B. D.; States, D. J.; Swaminathan, S.; Karplus, M.; *J. Comput. Chem.* **1983**, *4*, 187. [Crossref]
33. *Discovery Studio Modeling Environment*, Release 4.5. BIOVIA; Dassault Systèmes, San Diego, CA, USA, 2015.
34. Protein Data Bank (PDB), https://www.rcsb.org/structure/2J3N, accessed in August 2024.
35. Olmstead, A. W.; LeBlanc, G. A.; *Environ. Health Perspect.* **2003**, *111*, 919. [Crossref]
36. Ramos, R.; Costa, J.; Silva, R.; da Costa, G.; Rodrigues, A.; Rabelo, E.; Souto, R.; Taft, C.; Silva, C.; Rosa, J.; Santos, C.; Macêdo, W.; *Pharmaceuticals* **2019**, *12*, 20. [Crossref]
37. Trott, O.; Olson, A. J.; *J. Comput. Chem.* **2010**, *31*, 455. [Crossref]
38. Hollingsworth, S. A.; Dror, R. O.; *Neuron* **2018**, *99*, 1129. [Crossref]
39. Ononamadu, C. J.; Abdalla, M.; Ihegboro, G. O.; Li, J.; Owolarafe, T. A.; John, T. D.; Tian, Q.; *Biochem. Biophys. Rep.* **2021**, *28*, 101178. [Crossref]
40. Phillips, J. C.; Hardy, D. J.; Maia, J. D. C.; Stone, J. E.; Ribeiro, J. V.; Bernardi, R. C.; Buch, R.; Fiorin, G.; Hénin, J.; Jiang, W.; McGreevy, R.; Melo, M. C. R.; Radak, B. K.; Skeel, R. D.; Singharoy, A.; Wang, Y.; Roux, B.; Aksimentiev, A.; Luthey-Schulten, Z.; Kalé, L. V.; Schulten, K.; Chipot, C.; Tajkhorshid, E.; *J. Chem. Phys.* **2020**, *153*, 44130. [Crossref]
41. Case, D. A.; Aktulga, H. M.; Belfon, K.; Cerutti, D. S.; Cisneros, G. A.; Cruzeiro, V. W. D.; Forouzesh, N.; Giese, T. J.; Götz, A. W.; Gohlke, H.; Izadi, S.; Kasavajhala, K.; Kaymak, M. C.; King, E.; Kurtzman, T.; Lee, T. S.; Li, P.; Liu, J.; Luchko, T.; Luo, R.; Manathunga, M.; Machado, M. R.; Nguyen, H. M.; O'Hearn, K. A.; Onufriev, A. V.; Pan, F.; Pantano, S.; Qi, R.; Rahnamoun, A.; Risheh, A.; Schott-Verdugo, S.; Shajan, A.; Swails, J.; Wang, J.; Wei, H.; Wu, X.; Wu, Y.; Zhang, S.; Zhao, S.; Zhu, Q.; Cheatham, T. E.; Roe, D. R.; Roitberg, A.; Simmerling, C.; York, D. M.; Nagan, M. C.; Merz, K. M.; *J. Chem. Inf. Model.* **2023**, *63*, 6183. [Crossref]
42. Antolínez, S.; Jones, P. E.; Phillips, J. C.; Hadden-Perilla, J. A.; *J. Chem. Inf. Model.* **2024**, *64*, 543. [Crossref]
43. Maier, J. A.; Martinez, C.; Kasavajhala, K.; Wickstrom, L.; Hauser, K. E.; Simmerling, C.; *J. Chem. Theory Comput.* **2015**, *11*, 3696. [Crossref]
44. Sprenger, K. G.; Jaeger, V. W.; Pfaendtner, J.; *J. Phys. Chem. B* **2015**, *119*, 5882. [Crossref]
45. Yousaf, N.; Alharthy, R. D.; Maryam; Kamal, I.; Saleem, M.; Muddassar, M.; *PeerJ* **2023**, *11*, 14936. [Crossref]
46. Bastos, R. S.; de Lima, L. R.; Neto, M. F. A.; Maryam; Yousaf, N.; Cruz, J. N.; Campos, J. M.; Kimani, N. M.; Ramos, R. S.; Santos, C. B. R.; *Int. J. Mol. Sci.* **2023**, *24*, 8814. [Crossref]
47. Humphrey, W.; Dalke, A.; Schulten, K.; *J. Mol. Graphics* **1996**, *14*, 33. [Crossref]
48. Roe, D. R.; Cheatham, T. E.; *J. Chem. Theory Comput.* **2013**, *9*, 3084. [Crossref]
49. *R Foundation for Statistical Computing*, R Core Team, Vienna, Austria, 2021. [Link] accessed in August 2024
50. Silva, L.; Ferreira, E.; Maryam; Espejo-Román, J.; Costa, G.; Cruz, J.; Kimani, N.; Costa, J.; Bittencourt, J.; Cruz, J.; Campos, J.; Santos, C.; *Molecules* **2023**, *28*, 1035. [Crossref]
51. Sun, H.; Li, Y.; Shen, M.; Tian, S.; Xu, L.; Pan, P.; Guan, Y.; Hou, T.; *Phys. Chem. Chem. Phys.* **2014**, *16*, 22035. [Crossref]
52. Han, Y.; Zhang, J.; Hu, C. Q.; Zhang, X.; Ma, B.; Zhang, P.; *Front. Pharmacol.* **2019**, *10*, 1. [Crossref]
53. Lohidakshan, K.; Rajan, M.; Ganesh, A.; Paul, M.; Jerin, J.; *Bangladesh J. Pharmacol.* **2018**, *13*, 23. [Crossref]
54. Pawar, S. S.; Rohane, S. H.; *Asian J. Res. Chem.* **2021**, *14*, 1. [Crossref]

55. Yang, Y.; Shi, C. Y.; Xie, J.; Dai, J. H.; He, S. L.; Tian, Y.; *Molecules* **2020**, *25*, 189. [Crossref]
56. Sun, B.; Zhang, H.; Liu, M.; Hou, Z.; Liu, X.; *MedChemComm* **2018**, *9*, 1178. [Crossref]
57. Yadav, D. K.; Kumar, S.; Saloni; Misra, S.; Yadav, L.; Teli, M.; Sharma, P.; Chaudhary, S.; Kumar, N.; Choi, E. H.; Kim, H. S.; Kim, M.; *Sci. Rep.* **2018**, *8*, 4777. [Crossref]
58. Singh, R.; Balupuri, A.; Sobhia, M. E.; *Mol. Simul.* **2013**, *39*, 49. [Crossref]
59. Banerjee, P.; Eckert, A. O.; Schrey, A. K.; Preissner, R.; *Nucleic Acids Res.* **2018**, *46*, 257. [Crossref]
60. Xu, C.; Cheng, F.; Chen, L.; Du, Z.; Li, W.; Liu, G.; Lee, P. W.; Tang, Y.; *J. Chem. Inf. Model.* **2012**, *52*, 2840. [Crossref]
61. Gowthaman, U.; Jayakanthan, M.; Sundar, D.; *BMC Bioinf.* **2008**, *9*, 14. [Crossref]
62. Ramos, R. S.; Borges, R. S.; de Souza, J. S. N.; Araujo, I. F.; Chaves, M. H.; Santos, C. B. R.; *Int. J. Mol. Sci.* **2022**, *23*, 1781. [Crossref]
63. Ribeiro, A. N.; Lopes, S. Q.; Marinho, V. H. S.; Araújo, I. F.; Ramos, R. S.; Souto, R. N. P.; Oliveira, A. N.; Luque, R.; Nascimento, L. A.; Ferreira, I. M.; *Waste Biomass Valorization* **2023**, *12*, 3367. [Crossref]
64. Kim, I. H.; Pham, V.; Jablonka, W.; Goodman, W. G.; Ribeiro, J. M. C.; Andersen, J. F.; *J. Biol. Chem.* **2017**, *292*, 15329. [Crossref]
65. Wang, J.; Murphy, E. J.; Nix, J. C.; Jones, D. N. M.; *Sci. Rep.* **2020**, *10*, 3300. [Crossref]
66. Bittova, L.; Jedlicka, P.; Dracinsky, M.; Kirubakaran, P.; Vondrasek, J.; Hanus, R.; Jindra, M.; *J. Biol. Chem.* **2019**, *294*, 410. [Crossref]
67. Alomar, A. A.; Eastmond, B. H.; Alto, B. W.; *Sci. Rep.* **2021**, *11*, 21062. [Crossref]
68. Riddiford, L. M.; *J. Insect Physiol.* **2008**, *54*, 895. [Crossref]
69. Wang, Y.; Guo, Y.; Qiang, S.; Jin, R.; Li, Z.; Tang, Y.; Leung, E. L. H.; Guo, H.; Yao, X.; *Front. Pharmacol.* **2021**, *12*, 1. [Crossref]

Submitted: February 25, 2024
Published online: August 13, 2024